Materials Science & Engineering C 110 (2020) 110705

Contents lists available at ScienceDirect

Materials Science & Engineering C

journal homepage: www.elsevier.com/locate/msec

# Injectable double-crosslinked hydrogels with kartogenin-conjugated polyurethane nano-particles and transforming growth factor β3 for *in-situ* cartilage regeneration

Wenshuai Fan[a,1], Liu Yuan[b,c,1], Jinghuan Li[d,1], Zhe Wang[a], Jifei Chen[a], Changan Guo[a], Xiumei Mo[b,c,**], Zuoqin Yan[a,*]

[a] Department of Orthopedics, Zhongshan Hospital, Fudan University, Shanghai 200032, China
[b] Biomaterials and Tissue Engineering Lab, College of Chemistry, Chemical Engineering and Biotechnology, Donghua University, Shanghai 201620, China
[c] State Key Laboratory for Modification of Chemical Fibers and Polymer Materials, College of Materials Science and Engineering, Donghua University, Shanghai 201620, China
[d] Department of Hepatic Oncology, Liver Cancer Institute, Zhongshan Hospital, Fudan University, Shanghai 200032, China

ARTICLE INFO

*Keywords:*
Cartilage repair
*In-situ* regeneration
Functional hydrogel
Kartogenin
TGF-β3

ABSTRACT

Articular cartilage has a limited ability for self-repair after injury. Implantation of scaffolds functionalized with bioactive molecules that could induce the migration and chondrogenesis of endogenous mesenchymal stem cells (MSCs) provides a convenient alternative for *in-situ* cartilage regeneration. In this study, we found the synergistic effects of kartogenin (KGN) and transforming growth factor β3 (TGF-β3) on chondrogenesis of MSCs *in vitro*, indicating that KGN and TGF-β3 are a good match for cartilage regeneration. Furthermore, we confirmed that KGN promoted the chondrogenesis of MSCs through attenuating the degradation of Runx1, which physically interacted with p-Smad3 in nuclei of MSCs. Meanwhile, we designed an injectable double-crosslinked hydrogel with superior mechanical property and longer support for cartilage regeneration by modifying sodium alginate and gelatin. When loaded with KGN conjugated polyurethane nanoparticles (PN-KGN) and TGF-β3, this hydrogel showed biological functions by the release of KGN and TGF-β3, which promoted the MSC migration and cartilage regeneration in one system. In conclusion, the cell-free hydrogel, along with PN-KGN and TGF-β3, provides a promising strategy for cartilage repair by attracting endogenous MSCs and inducing chondrogenesis of recruited cells in a single-step procedure.

## 1. Introduction

The articular cartilage defect is a common disease in the clinic and an increasing health care concern. As the articular cartilage is avascular and low cellular tissue that has a limited spontaneous regeneration after injury, the repair of cartilage defects is a considerable challenge [1]. Although several methods, such as microfracture or mosaicplasty, have been developed to treat cartilage defects, the results have largely been unsatisfactory [2]. Tissue engineering is a promising therapeutic modality for cartilage regeneration, which seeks to improve cartilage repair by introducing cartilage-forming cells on supporting scaffolds [3]. Mesenchymal stem cells (MSCs) are suitable cells for regeneration with pluripotent capabilities [4]. Compared to cell delivery, implantation of cell-free scaffolds functionalized with bioactive molecules that could induce the migration and differentiation of endogenous MSCs provides a convenient alternative for *in-situ* cartilage regeneration [5].

Bioactive molecules play essential roles in regulating cell behaviors, such as proliferation, migration, and differentiation. Transforming growth factor β (TGF-β) is frequently used to induce chondrogenesis. Also, it is reported that TGF-β showed an effect on improving MSC homing [6]. However, TGF-β induced the osteoarthritis-like change of cartilage [7]. Recently, kartogenin (KGN), a heterocyclic compound selected from 22,000 drug-like molecules using an image-based high-throughput screen system, was reported to have both regenerative and protective effects on cartilage [8]. Xu et al. reported that intra-articular injection of KGN could enhance the quality of full-thickness cartilage defect repair after microfracture, with better defect filling and increased hyaline-like cartilage formation [9]. In our previous study, we

* Correspondence to: Zuoqin Yan, Department of Orthopedics, Zhongshan Hospital, Fudan University, Shanghai 200032, China.
** Corresponding author.
*E-mail addresses:* xmm@dhu.edu.en (X. Mo), yan1002@hotmail.com (Z. Yan).
[1] These authors contributed equally to this work.

https://doi.org/10.1016/j.msec.2020.110705
Received 3 November 2019; Received in revised form 28 December 2019; Accepted 28 January 2020
Available online 28 January 2020
0928-4931/ 

developed KGN-conjugated polyurethane nanoparticles (PN-KGN) that could control the release of KGN and attenuate the degeneration of cartilage [10]. Combined application of KGN and TGF-β may better promote cartilage regeneration in one system.

Hydrogels have obtained more attention in cartilage tissue engineering due to their similar properties to cartilage extracellular matrix with high water content [11]. Besides, hydrogels can incorporate cells or bioactive molecules, serving as a spatial structure for cell proliferation and differentiation or utilized as a suitable delivery vehicle to release bioactive molecules [12,13]. Injectable hydrogels will more facilitate surgical procedures in the clinic because they show minimal invasion and can form any desired shape to match irregular defects [14]. In recent years, various hydrogels have been fabricated for cartilage regeneration, including natural or synthetic materials. However, conventional hydrogels are constructed based on single crosslink, leading to the scaffolds with inferior mechanical properties [15]. In our previous study, we designed an injectable double-crosslinked hydrogel (AMSA/AG hydrogel) composed of two modified natural materials [16]. In this study, we further study how to realize its application in cartilage repair.

We firstly investigated the combined effects of KGN and TGF-β3 on chondrogenesis of MSCs *in vitro* and explored the potential mechanisms about the synergistic effect. Then we constructed biofunctionalized AMSA/AG hydrogels by encapsulating PN-KGN and TGF-β3 and evaluated its effect on MSCs migration and treatment for cartilage defects *in vivo*. We hypothesized that the hydrogel loading with PN-KGN and TGF-β3 could promote *in-situ* cartilage repair within a one-step surgical procedure by facilitating MSC recruitment and chondrogenesis.

## 2. Materials and methods

### 2.1. Cell relevant assays

For cell cytotoxicity, cell number was assessed by CCK-8 assay according to the manufacturer's instructions (Beyotime, China). For cell cycle, cells were fixed with −20 °C pre-cooled 70% ethanol overnight at 4 °C. After washed, 100 μL RNase A was added and incubated at 37 °C for 30 min, then 400 μL PI stain was added and incubated at 4 °C for 30 min. The stained cells were acquired in a flow cytometer (BD FACSAria™ II sorter) at an excitation wavelength of 488 nm. Data were processed using FlowJo software (FlowJo, Inc., USA). For cell migration, $10^5$ cells were seeded on the upper chamber of transwell plates (Corning, USA). Incubation at 37 °C for 8 h, the upper chamber was fixed with 4% formaldehyde and stained with 0.5% crystal violet for 10 min. After washed, the upper surface of chambers was carefully wiped by a cotton swab to remove the cells that had not migrated to the lower surface.

### 2.2. Chondrogenic differentiation

The pellet culture method was performed to induce chondrogenesis of MSCs. Briefly, $5 \times 10^5$ cells were centrifuged at 500*g* for 5 min in a centrifuge tube. Pellets cultured in basal chondrogenic medium were served as control group, contained 50 mg/mL ITS + Premix, 100 nM dexamethasone, 50 mg/L ascorbate-2-phosphate, 40 mg/L proline and 100 mg/L pyruvate (Cyagen Biosciences, USA). Control medium supplemented with 100 nM KGN, 10 ng/mL TGF-β3 or both was served as KGN, TGF-β or KGN + TGF-β group. After 4-week incubation, chondrogenesis was tested by hematoxylin-eosin (HE), Alcian blue, and collagen II (Col II) immunohistochemistry staining. The 1, 9-dimethyl methylene blue (DMMB) dye-binding assay was used for detecting the content of glycosaminoglycan (GAG). Relative gene expressions of aggrecan (AGG), Col II, and Sox9 were measured by reverse transcription-polymerase chain reaction (PCR).

### 2.3. Quantitative real-time PCR

Total RNA was extracted from cells using Trizol reagent (Invitrogen, USA). cDNA was obtained by reverse-transcription using PrimeScript RT Master Mix (Takara, Japan). Quantitative real-time PCR was performed using 2× SYBR Green PCR Master Mix using StepOnePlus™ Real-Time PCR System (Applied Biosystems, USA), under the following conditions: 95 °C for 30 s, followed by 40 cycles at 95 °C for 5 s, 60 °C for 34 s, and a melt cure step. The expression levels of target genes for each experiment were normalized to the internal control glyceraldehyde 3-phosphate dehydrogenase (GAPDH) and calculated by the $2^{-\Delta\Delta Ct}$ method. All experiments were performed in triplicates.

### 2.4. Western blot analysis

Cell lysates were extracted using RIPA lysis buffer containing PMSF and phosphatase inhibitor (Roche, Switzerland) at 4 °C. The extracts were prepared using cytoplasmic extraction reagents (Pierce, USA). Protein samples were separated by 10% SDS-PAGE gel and transferred onto polyvinylidene difluoride (PVDF) membranes (Millipore, USA). The membranes were blocked with 5% BSA for 1 h, washed, and then incubated with primary antibodies for p-Smad3, Smad3, Runx1, and tubulin (Abcam, UK) overnight at 4 °C. After washing, the membrane was incubated with HRP-conjugated secondary antibodies (Santa Cruz, USA) and detected using enhanced chemiluminescence method. The protein expressions were quantified using densitometry with ImageJ software (National Institutes of Health, USA) and normalized to relative tubulin expressions. All experiments were performed in triplicates.

### 2.5. MSC transfection

MSCs were transfected with either control lentiviral vectors or Runx1 shRNA lentiviral vectors established by Genechem Biotechnology (China), as described in the instructions. Three Runx1 specific target sequences were chosen and the efficiency of Runx1 knockdown was assessed by Western blot.

### 2.6. Immunofluorescence

Cells were treated with 4% formaldehyde and then permeabilized with 0.5% Triton X-100. Non-specific block binding was carried out with 5% BSA before incubation with primary antibodies for p-Smad3 and Runx1 at 1:100 dilutions overnight at 4 °C. After washing, incubated with secondary antibodies (Invitrogen) at 37 °C for 1 h. Nuclei were stained with DAPI (Roche) for 10 min. Fluorescence microscopy (Leica Microsystems Imaging Solutions, UK) was used to observe the results.

### 2.7. Co-immunoprecipitation (co-IP)

Co-IP was done using the Pierce co-IP kit following the manufacturer's protocol. Briefly, the primary antibody was immobilized for 2 h using the amino-link plus coupling resin or the negative control agarose resin, respectively. The control resin is not amine-reactive, preventing covalent immobilization of the primary antibody onto the resin. The resins were then washed and incubated with cell lysates overnight at 4 °C with gentle mixing. After washed the resins, the samples were eluted using the elution buffer and analyzed by Western blot.

### 2.8. Synthesis of aldehyde methylene sodium alginate (AMSA) and amino gelatin (AG)

AMSA and AG were prepared as previously described [16]. Briefly, sodium alginate was oxidized with sodium periodate to obtain aldehyde sodium alginate (ASA). ASA was reacted with 2-aminoethyl methacrylate through N-(3-dimethyl aminopropyl)-N′-ethyl carbodiimide

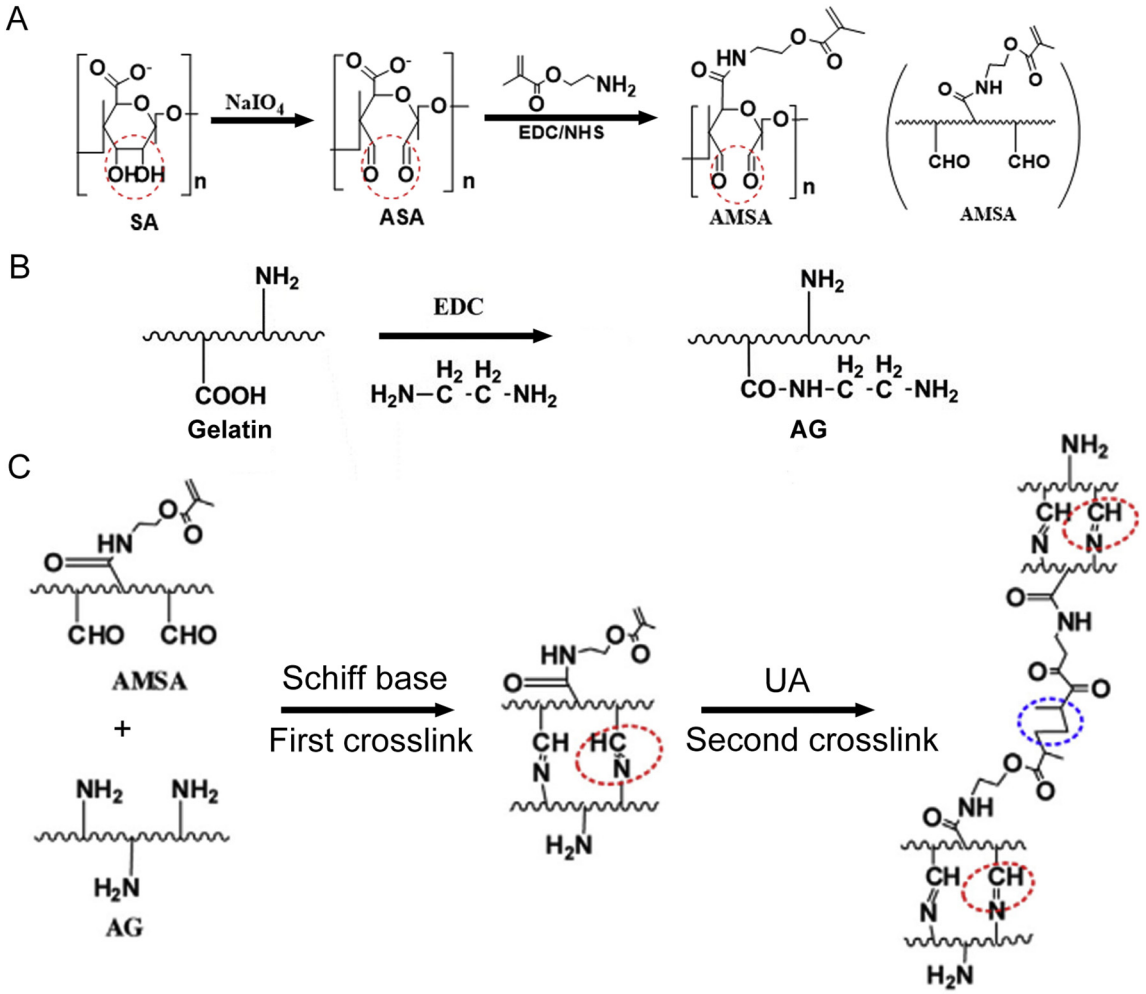


**Scheme 1.** Illustration of procedures to synthesize AMSA/AG hydrogels. (A) Preparation of AMSA. (B) Modification of AG. (C) Formation of injectable double-crosslinked hydrogels.

hydrochloride (EDC)/N-hydroxysuccinimide (NHS) condensation reaction to obtain AMSA. Gelatin was reacted with ethane diamine to obtain AG. The lyophilized AMSA was sterilized by ethylene oxide and AG was sterilized by UV irradiation.

### 2.9. Characterizations of AMSA/AG hydrogels

To fabricate hydrogels, AMSA, AG, and photoinitiator (Irgacure-2959) solutions were mixed. The first crosslink was formed *via* the Schiff based reaction between aldehyde groups in AMSA and amino groups in AG. The secondary crosslink was formed when irradiated by UV light at 365 nm (Scheme 1, Table 1). Polymer chemical structures were examined by Fourier transform infrared spectroscopy (FTIR; Nicolet 6700, Thermo Scientific, USA). The morphology of single or double crosslinked hydrogel was observed by scanning electron microscopy (SEM; JSM-5600, JEOL, Japan). The mechanical behavior was detected by compression tests using a material testing instrument (DXLL-20000, Instron, USA) at a strain rate of 10 mm/min. The degradation was monitored by measuring the weight remaining of hydrogels in PBS or 2 U/mL collagenase solution.

**Table 1**
The equilibrium swelling ratio and water absorption of single or double crosslinked hydrogels in PBS overnight at 37 °C.

| | Equilibrium swelling ratio | Equilibrium water absorption |
|---|---|---|
| Single-crosslinked hydrogel | 4.0 ± 0.7 | (79 ± 4)% |
| Double-crosslinked hydrogel | 2.5 ± 0.2 | (72 ± 2)% |

### 2.10. Synthesis of KGN conjugated polyurethane nanoparticles (PN-KGN)

As described in our previous study [10], polyurethane (PN) was synthesized from poly-(ethylene glycol) (PEG), hexamethylene diisocyanate (HDI) and N-BOC-Serinol with a molar ratio of 1:2:1. KGN was grafted to PN through EDC/NHS condensation reaction. The loading efficiency of KGN is 14%.

### 2.11. In vitro release study

PN-KGN or bovine serum albumin (BSA) encapsulated hydrogels were placed in saline at 37 °C in a shaking incubator (100 rpm). The saline was collected and refreshed at each sampling time point. The amounts of released KGN were measured by reverse-phase high-performance liquid chromatography (HPLC; 600E-2487, Waters, USA) spectrum using a C-18 column (150 × 4.6 mm, 5 μm). The amounts of released BSA were assessed by the BCA kit according to the manufacturer's instructions (Beyotime).

### 2.12. Animals and study design

Animals were provided by the Animal Research Committee of Zhongshan Hospital, Fudan University. All procedures were carried out according to the guide for the care and use of lab animals. A medial para-patellar incision was made to expose the articular surface. Osteochondral defects (6 mm diameter in New Zealand rabbits) were created at the center of the trochlear groove. The rabbits were randomized into three groups: control group, defects without any implantation; hydrogel group, implanted with pure hydrogels; and experiment group, implanted with hydrogels that contained 1.2 mg/mL PN-KGN and 100 ng/mL TGF-β3. Rabbits were sacrificed for analysis at 4, 8, and 12 weeks (n = 6).

### 2.13. Macroscopic examination

After euthanasia, knee joints were fully exposed without damaging the cartilage. The International Cartilage Repair Society (ICRS) macroscopic score was utilized by two independent observers blinded to experimental groups to assess repair results [17].

### 2.14. Histology

The dissected samples were fixed in 4% paraformaldehyde for 2 d and then decalcified in 10% EDTA for 8 weeks. After serial dehydration, the joints were embedded in paraffin and sagittally sectioned at 5 μm thickness. The sections were stained with HE and safranin-O/fast green. The O'Driscoll histology score was used by two observers blinded to evaluate the quality of repaired tissues [18]. For immunohistochemistry, anti-type II collagen antibodies (Novus, USA) were used as primary antibodies (1:100).

### 2.15. Statistical analysis

All data were expressed as mean ± standard deviation (SD). Statistical analyses were performed using GraphPad Prism (GraphPad Software Inc., USA). One-way analysis of variance (ANOVA) was used to assess group differences. $p < 0.05$ was considered statistically significant from at least three independent experiments.

## 3. Results and discussion

### 3.1. Synergistic effects of KGN and TGF-β3 on chondrogenesis of MSCs

A combination of bioactive molecules is an efficient strategy to enhance synergistic effects [19]. Liu et al. observed that the content of lubricin from BMSCs was the highest when treated with TGF-β1, BMP-7 and KGN [20]. In this study, we chose KGN and TGF-β3 to detect their effects on the chondrogenesis of MSCs. We first evaluated the cytotoxicity of KGN on MSCs and observed that KGN had no obvious cytotoxicity on MSCs at indicated concentrations. Cell cycle analysis also validated that KGN had no obvious effect on the population of MSCs in different phases of the cell cycle (Fig. S1). After pellet culture, the addition of KGN or TGF-β3 increased the secretion of AGG and Col II compared to the control. More importantly, the addition of KGN together with TGF-β3 resulted in a significant increase in the secretion of AGG and Col II, with bigger pellets and stronger staining of Alcian blue and immune-histochemistry for AGG and Col II (Fig. 1A). The content of GAG was quantitative analysis by DMMB assay, which showed that the addition of KGN together with TGF-β3 induced the most GAG synthesis (Fig. 1B). Meanwhile, the expression of cartilage-specific genes (AGG, Col II, and Sox9) was significantly increased with the addition of KGN together with TGF-β3, as compared to the cells treated with KGN or TGF-β3 alone (Fig. 1C). These results indicated the synergistic effects of KGN and TGF-β3 on the chondrogenesis of MSCs.

### 3.2. Potential mechanisms about synergistic effects of KGN and TGF-β3 on chondrogenesis

To determine the potential mechanism about the synergistic effects of KGN and TGF-β3 on chondrogenesis, we detected the down signaling molecule Smad3 and Runx1 that are crucial transcription factors for chondrogenesis [21]. As shown in Fig. 2A, the addition of TGF-β3 significantly increased levels of phosphorylated Smad3 as compared to the control while the addition of KGN did not change levels of phosphorylated Smad3. It is consistent with a previous study that TGF-β3 promotes the chondrogenesis of MSCs by activating Samd2/3 [22], and indicates that the effect of KGN on MSC chondrogenesis is not through directly phosphorylating Smad3. However, the protein level of Runx1 increased with the presence of KGN. The depletion of Runx1 significantly attenuated the expressions of AGG and Col II in the presence of KGN (Fig. S2). We detect the expression of Runx1 with the presence of KGN, and no distinct change was found in the mRNA level of Runx1. Whereas the protein degradation of Runx1 was extended in the presence of KGN, suggesting that KGN may participate in regulating Runx1 stability but not increasing its expression (Fig. 2B). KGN was reported to block the interaction between filamin A and CBFβ [8]. When dissociating from filamin A, CBFβ translocates into the nucleus and binds Runx family members [23]. CBFβ deficiency in osteoblasts and chondrocytes caused decreased protein levels of Runx2 by accelerating polyubiquitination-mediated proteasomal degradation [24,25]. *In vivo* study also exhibited that CBFβ regulates bone development by stabilizing Runx family proteins [26]. Runx1 was barely detected in CBFβ−/− mouse [27]. Taken together, we think that KGN promotes the chondrogenesis of MSCs by attenuating the degradation of Runx1.

Considering the optimal chondrogenesis of p-Smad3 and Runx1 co-existence, we further detected the interaction between p-Smad3 and Runx1 in MSCs. We performed immunofluorescence and observed the co-localization of these two proteins concentrated in cell nuclei (Fig. 2C). Co-immunoprecipitation assays also verified the interaction between p-Smad3 and Runx1. It showed that Runx1 was immunoprecipitated with p-Smad3 (Fig. 2D). In nuclei, phosphorylated Smads interact with various transcription factors, leading to a wide range of biological activities. Runx family members have been shown to work as co-transcription factors in Smad-mediated gene expressions [28]. Cooperation between Smad and Runx has been most documented in bone formation. Smadl/5 physically interact with Runx2 and synergistically induce the osteogenesis of MSCs [29]. Smad3 interacts with Runx2 and inhibit osteoblast-specific gene expressions [30]. As the optimal chondrogenesis of p-Smad3 and Runx1 co-existence, we confirmed the physical interaction between p-Smad3 and Runx1 in nuclei of MSCs.

### 3.3. Characterizations of AMSA/AG hydrogels

Hydrogels are three-dimensional crosslink networks that provide an appropriate microenvironment similar to the cartilage matrix. In our previous study, we fabricated an injectable hydrogel by modifying sodium alginate and gelatin [31]. However, the hydrogel, based on single crosslink, generally resulted in constructs with inferior mechanical properties that hindered the extensive application for load-bearing tissue [32]. Here, we developed it by further grafting methacrylate groups on ASA to fabricate a double-crosslinked hydrogel. Successful modifications of AMAS and AG were characterized by FTIR (Fig. S3). The mechanical test showed that the compressive stress-strain curve of double-crosslinked hydrogels was obviously improved compared to that of single-crosslinked hydrogels (Fig. 3A). The weight remaining of hydrogels indicated that double crosslinked hydrogels showed slower degradation (Fig. 3B). No cytotoxicity of double-crosslinked hydrogels was observed after cells were exposed to the hydrogel for 4 and 7 days (Fig. S6).

To fully reconstruct the damaged cartilage, it is important to

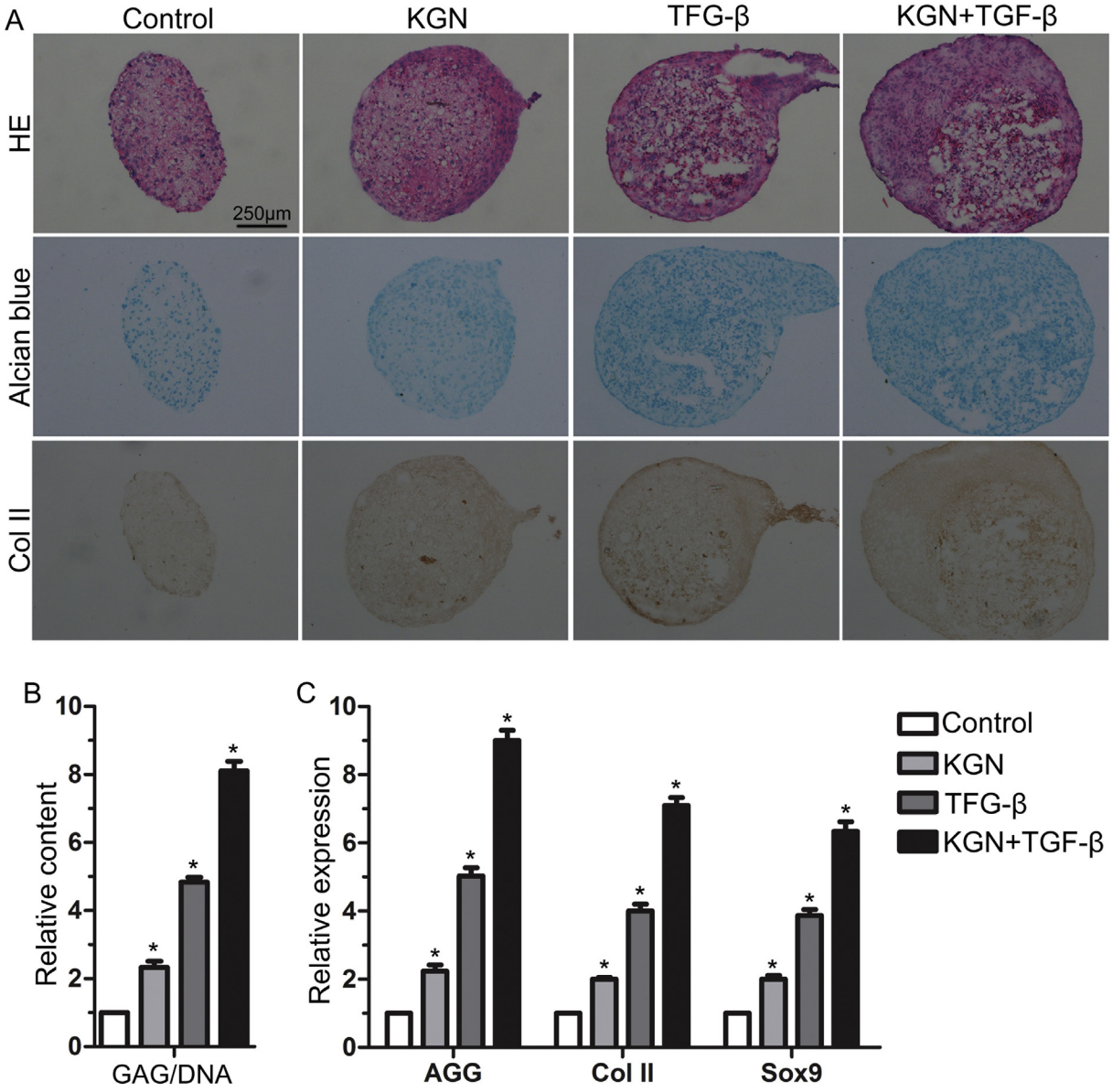


**Fig. 1.** Synergistic effects of KGN and TGF-β3 on chondrogenesis of MSCs *in vitro*. (A) HE, Alcian blue, and Col II immunohistochemistry staining for chondrogenesis of MSCs after pellet culture of 28 days, bar = 250 μm. The relative content of GAG (B) and relative expression of AGG, Col II, and Sox9 (C) in Control, KGN, TGF-β, and KGN + TGF-β group, n = 3, data were shown as mean ± SD, $^*p < 0.05$. (For interpretation of the references to colour in this figure legend, the reader is referred to the web version of this article.)

synthesize biocompatible scaffolds that mimic specific features of the native tissue and provide support to the newly formed tissue [33]. In our study, sodium alginate and gelatin are used because these two natural materials are cheap and easy to be obtained. Besides, sodium alginate and gelatin are easily modified to gain functional groups [34]. However, sodium alginate is not biodegradable. It is reported that its aldehyde derivative is biodegradable [35]. Therefore, we oxidized sodium alginate with sodium periodate to make it biodegradable. The biodegradable of hydrogels avoids the residual of implants *in vivo*. The viscosity is a parameter for the gel to have injectable property [34]. And the gelling of aqueous media under mild conditions at a proper rate is crucial for the application of injectable hydrogel. Our hydrogel is crosslinked by two moderate reactions to form *in-situ* hydrogels with a suitable gelation time. The first crosslink was quickly formed through Schiff base reaction in 120 s, making the mixtures shape and retain at cartilage defects. The second crosslink was formed through photo crosslink, making the hydrogels show improved mechanical properties [16]. Recently, the double-crosslinked principle is a proven and universal method for creating strong and tough hydrogels, expanding the choice for designing next-generation orthopedic implants [36,37]. Our injectable double-crosslinked hydrogels provide a promising scaffold for cartilage tissue engineering.

### 3.4. Biofunctionalized AMSA/AG hydrogels with KGN and TGF-β3

As the synergistic effect of KGN and TGF-β3 on chondrogenesis of MSCs, we further biofunctionalized AMSA/AG hydrogels by encapsulating KGN and TGF-β3. The release study showed the quick release of BSA from the hydrogel when BSA was encapsulated directly. To slow down the release of KGN, we encapsulated PN-KGN instead of KGN in the hydrogels (Fig. 4A). The incorporation of PN-KGN had no significant effects on the mechanical properties of the hydrogel (Fig. S7). SEM image showed that the hydrogel still maintained interconnecting porous structures and PN-KGN were distributed in the

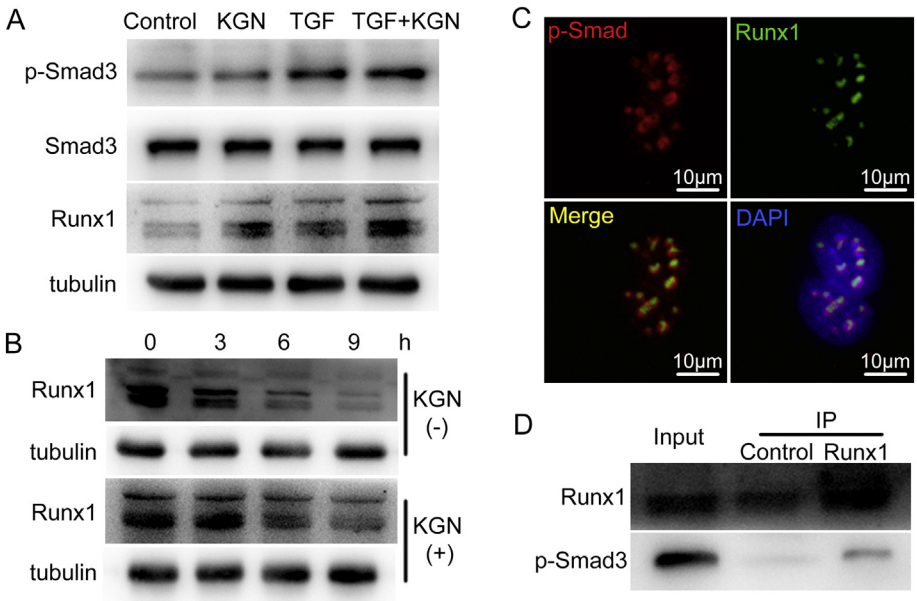


**Fig. 2.** Effects of KGN and TGF-β3 on Smad3 and Runx1. (A) The protein levels of p-Smad3, Smad3, and Runx1 in Control, KGN, TGF-β3, and KGN + TGF-β3 group. (B) After treated with cycloheximide (50μg/mL), the protein levels of Runx1 with or without the presence of KGN at 0, 3, 6, and 9 h. (C) Immunofluorescence for the co-localization of p-Smad3 (red) and Runx1 (green) in nuclei (blue) of MSCs, bar = 10 μm. (D) The interaction of p-Smad3 and Runx1 detected by co-immunoprecipitation. (For interpretation of the references to colour in this figure legend, the reader is referred to the web version of this article.)

hydrogel (Fig. 4B). More importantly, the hydrogels showed a chemotactic effect on MSCs through releasing TGF-β3 (Figs. 5, S8). *In situ* forming hydrogels loaded with cells or bioactive molecules are usually used to enhance tissue regeneration [38,39]. Compared to hydrogels loaded with cells, hydrogels loaded with bioactive molecules are more convenient modalities to achieve tissue repair with simplified procedures, reduced time and expense [40]. It will cause burst release when a hydrogel is loaded with biomolecules directly [41]. The direct loading of TGF-β3 caused the burst release of TGF-β3, which is helped to recruit endogenous MSCs rapidly. Microsphere encapsulation is an effective method to avoid the burst release of biomolecules. The gradual release of KGN could contribute to maintaining cartilage protection [42].

### *3.5. Cartilage repair assessment of PN-KGN and TGF-β3 encapsulated hydrogels*

To evaluate the repair effect of PN-KGN and TGF-β3 encapsulated hydrogels on large cartilage defects (6 mm in diameter) *in vivo*, full-thickness cartilage defects were created at the center of the trochlear groove in rabbits. The gross appearance of cartilage repair was evaluated in each group at 4, 8, and 12 weeks. At 4 weeks, although the defects were still distinct in all groups, the defects in the experiment group began to cover with somewhat white cartilage-like tissue while the defects in the control and hydrogel group were only filled with reddish tissues. At 8 weeks, the defects in the experiment group were nearly full filled with regenerative tissue, while the defects in the control and hydrogel group were just partially covered by uneven neotissue. At 12 weeks, the defects in the experiment group become indistinguishable, closer to the surrounding normal cartilage, while the defects in the control and hydrogel group were still obvious (Fig. 6A). Results of the ICRS macroscopic score revealed no differences between the control and hydrogel group. However, the experiment group acquired significantly higher scores than the other two groups (Fig. 6B). In histological observations, the defects in the control and hydrogel group were insufficiently filled with thin fibrous tissue at any time point. However, the defects in the experiment group were gradually repaired over time. At 12 weeks, the defects were sufficiently filled with hyaline-like cartilaginous tissue and regenerative tissues were well integrated with the adjacent tissues in the experiment group (Fig. 7A). For the O'Driscoll histology score, the experimental group obtained high scores related to multiple aspects, such as surface regularity, thickness, and structural integrity (Fig. 7B). The immunohistochemistry also showed intense and even staining for Col II in the experiment group (Fig. 8). Our results showed that the AMSA/AG hydrogels loaded with PN-KGN and TGF-β3 exhibited good performances for large cartilage defect repair *in vivo* without exogenous MSCs.

KGN has become a new additive for cartilage tissue engineering since it was reported to induce the chondrogenesis of MSCs and have both regenerative and protective effects on cartilage [43]. KGN was shown to effectively promote cartilage regeneration *in vivo* when it was

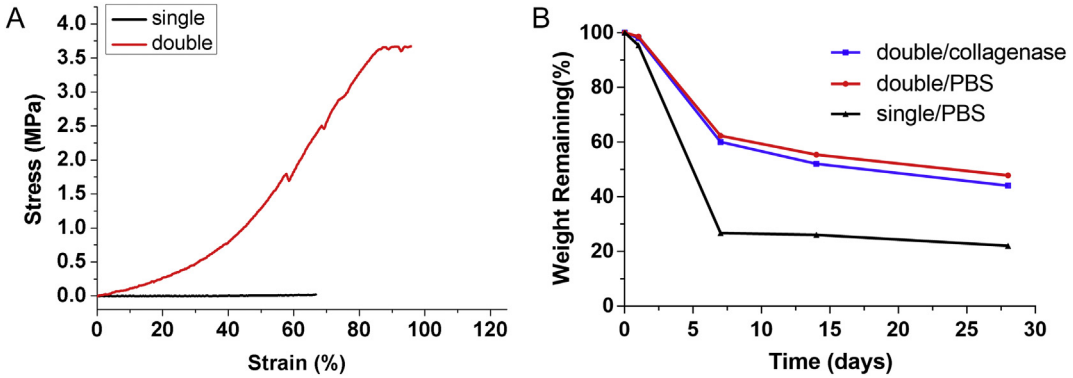


**Fig. 3.** Characterizations of AMSA/AG hydrogels. (A) The compressive stress-strain curves of single and double crosslinked hydrogels. (B) The degradation of single and double crosslinked hydrogels in PBS or 2 U/mL collagenase solution.

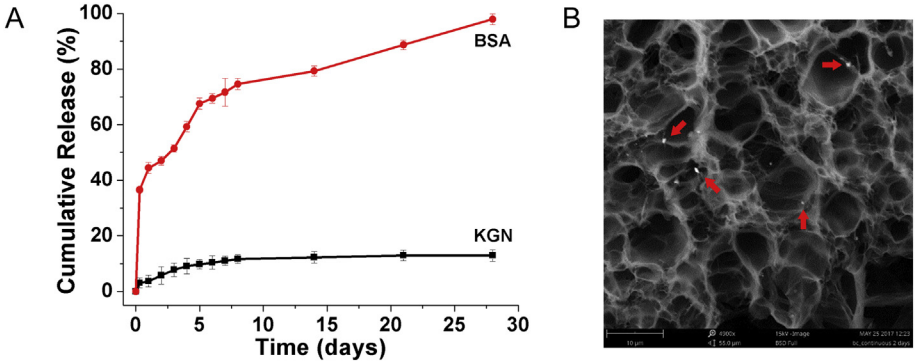


**Fig. 4.** (A) *In vitro* release of KGN and BSA from double-crosslinked hydrogels. (B) SEM image of double-crosslinked hydrogels with the incorporation of PN-KGN (red arrows). (For interpretation of the references to colour in this figure legend, the reader is referred to the web version of this article.)

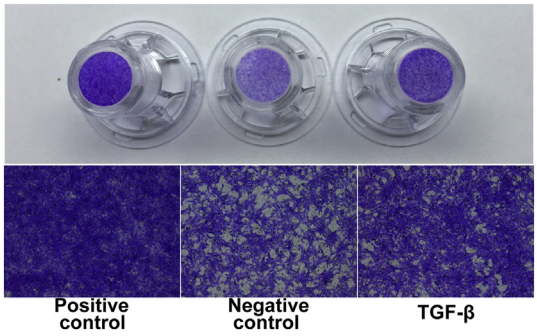


**Fig. 5.** The migration of MSCs in positive or negative control and AMSA/AG hydrogels that could release TGF-β3.

encapsulated in hydrogels with exogenous MSCs [39,44]. As mentioned above, the recruitment of MSCs to the defect site is a more convenient method for *in-situ* cartilage regeneration, which could also avoid the risk of infection due to *in vitro* cell culture. Based on a previous study [45], Shi et al. constructed a single-crosslinked hyaluronic acid hydrogel loaded with KGN-encapsulated PLGA nanoparticles for cartilage regeneration, we designed a double-crosslinked hydrogel and biofunctionalized it by encapsulating KGN and TGF-β3. The improved mechanical properties of double-crosslinked hydrogels could provide adequate support for cartilage regeneration. And the combination of KGN and TGF-β3 significantly increased the anabolism of aggrecan and collagen II. Recently, Jia et al. reported the synergistic effects of KGN and TGF-β3 on hyaline-like cartilage regeneration that KGN inhibited the hypertrophy induced by TGF-β3 when MSCs were intra-articular injection with KGN and TGF-β3 [46]. Meanwhile, Li et al. observed that hydrogels encapsulated with KGN and growth factors increased the expression of lubricin, an essential mucinous glycoprotein to prevent

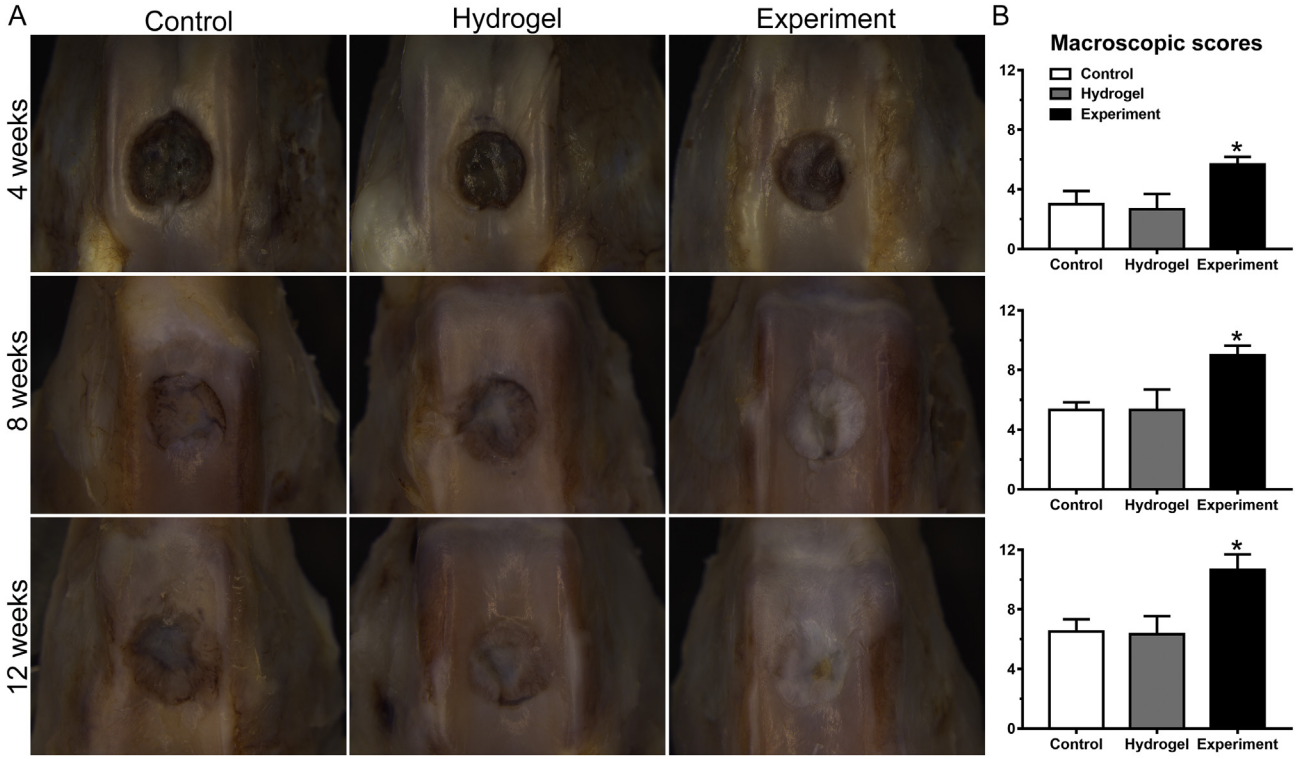


**Fig. 6.** Gross evaluations of cartilage repair. (A) Macroscopic views of cartilage repair at 4, 8, and 12 weeks after 6 mm defects created in three groups: Control group, defects were left without any implantation; Hydrogel group, implanted with pure hydrogels; and Experiment group, implanted with hydrogels that contained 1.2 mg/mL PN-KGN and 100 ng/mL TGF-β3. (B) The ICRS macroscopic scores of repaired cartilages at 4, 8, and 12 weeks, $^{*}p < 0.05$ *vs.* Control.

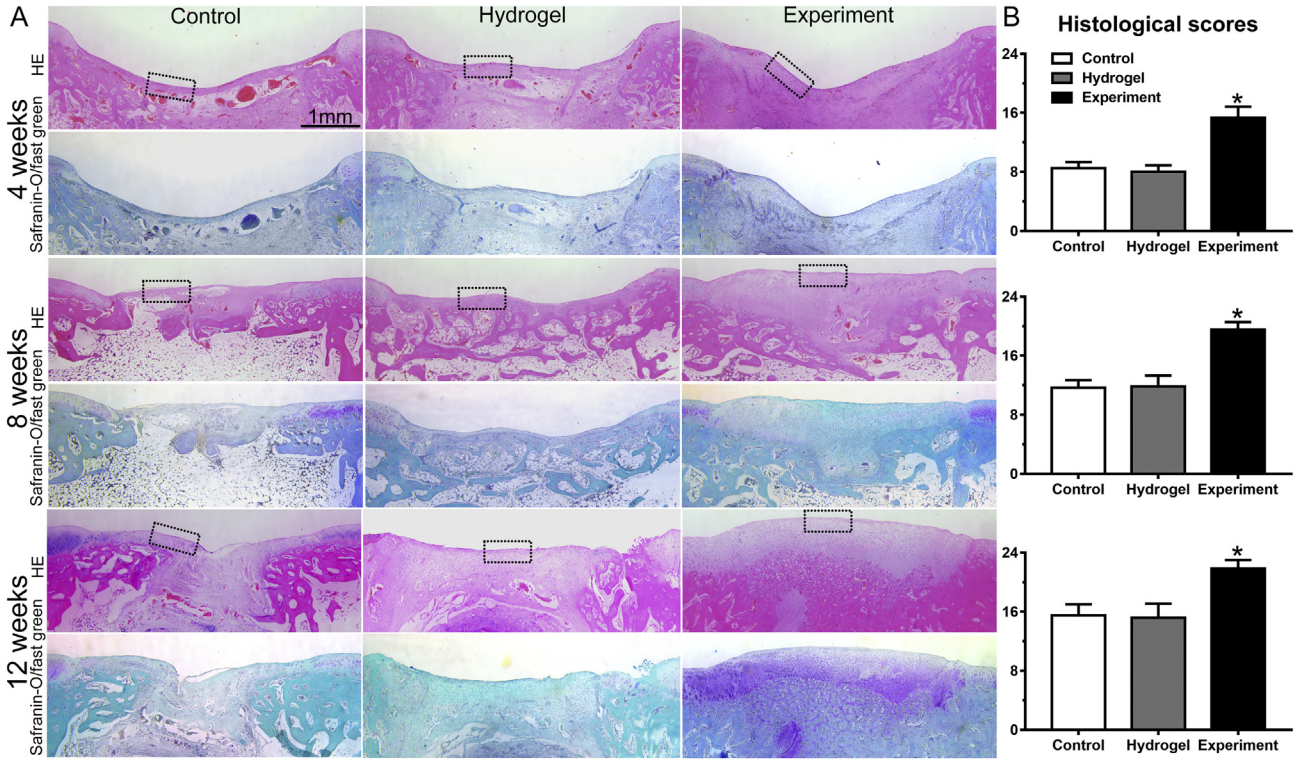


**Fig. 7.** Histological evaluations of cartilage repair. (A) HE and safranin-O/fast green staining of cartilage repair at 4, 8, and 12 weeks in Control, Hydrogel, and Experiment group, bar = 1 mm. (B) The O'Driscoll histology scores of repaired cartilages at 4, 8, and 12 weeks, $^{*}p < 0.05$ *vs.* Control. (For interpretation of the references to colour in this figure legend, the reader is referred to the web version of this article.)

cartilage degeneration [47]. These studies suggested that the combination of KGN and TGF-β3 could also be of great importance for osteoarthritis treatment.

## 4. Conclusion

In this study, we designed a cell-free hydrogel along with PN-KGN and TGF-β3 for cartilage repair by attracting endogenous MSCs and inducing chondrogenesis of recruited cells in one system. We found that KGN and TGF-β3 synergistically enhanced the chondrogenesis of MSCs and further confirmed that KGN promoted the chondrogenesis of MSCs through attenuating the degradation of Runx1, which physically interact with p-Smad3 in nuclei of MSCs. We developed an injectable double-crosslinked hydrogel with superior mechanical property and longer support for cartilage regeneration by modifying sodium alginate and gelatin. When loaded with PN-KGN and TGF-β3, the cell-free hydrogel showed bio-functions by the release of KGN and TGF-β3, which promoted the MSC migration and cartilage regeneration in a single-step procedure.

## CRediT authorship contribution statement

**Wenshuai Fan:** Methodology, Data curation, Writing - original draft. **Liu Yuan:** Methodology, Resources, Data curation. **Jinghuan Li:** Methodology, Writing - original draft, Funding acquisition. **Zhe Wang:** Data curation, Formal analysis. **Jifei Chen:** Validation, Formal analysis.

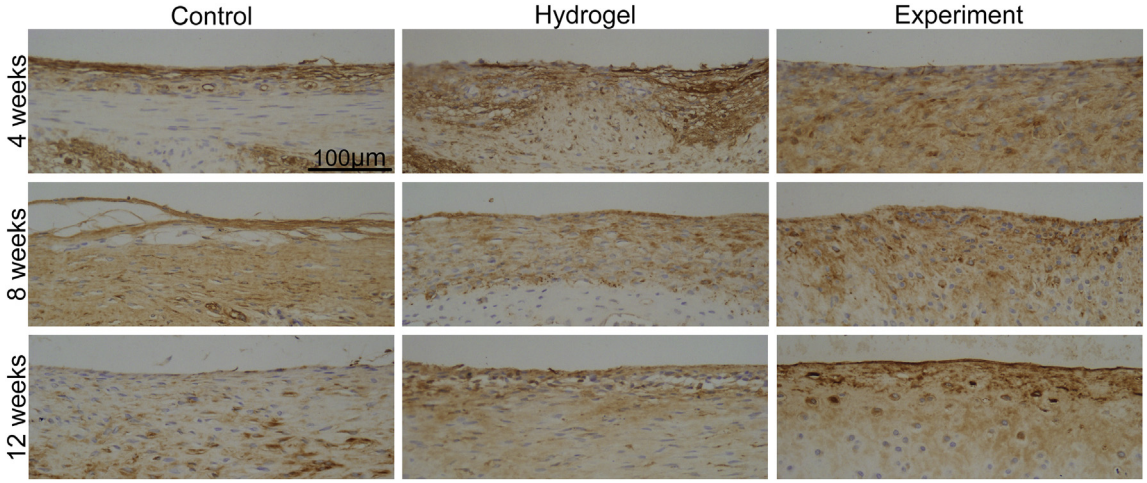


**Fig. 8.** Col II Immunohistochemistry staining for cartilage repair at 4, 8, and 12 weeks in Control, Hydrogel, and Experiment group, corresponding to the location of dashed rectangles in Fig. 7, bar = 100 μm.

**Changan Guo:** Validation, Investigation. **Xiumei Mo:** Conceptualization, Resources, Writing - review & editing. **Zuoqin Yan:** Conceptualization, Supervision, Writing - review & editing, Funding acquisition.

## Declaration of competing interest

The authors declare that they have no known competing financial interests or personal relationships that could have appeared to influence the work reported in this paper.

## Acknowledgements

This work was supported by the National Natural Science Foundation of China (Grant No. 81672157, 81871742, and 81802320) and Shanghai Hospital Development Center Emerging Advanced Technology Joint Research Project (Grant No. SHDC12017107).

## Appendix A. Supplementary data

Supplementary data to this article can be found online at https://doi.org/10.1016/j.msec.2020.110705.

## References

[1] D.J. Huey, J.C. Hu, K.A. Athanasiou, Unlike bone, cartilage regeneration remains elusive, Science 338 (2012) 917–921.
[2] E.A. Makris, A.H. Gomoll, K.N. Malizos, J.C. Hu, K.A. Athanasiou, Repair and tissue engineering techniques for articular cartilage, Nat. Rev. Rheumatol. 11 (2015) 21–34.
[3] W. Fan, Y. Wang, L. Yuan, S. Li, J. Pan, C. Chen, Z. Yan, C. Guo, Enhancing synovial mesenchymal stem cell adhesion and selection via an Avidin-Biotin-CD105 binding system for cartilage tissue engineering, J. Biomater. Tissue Eng. 6 (2016) 27–34.
[4] F. Barry, M. Murphy, Mesenchymal stem cells in joint disease and repair, Nat. Rev. Rheumatol. 9 (2013) 584–594.
[5] G.I. Im, Endogenous cartilage repair by recruitment of stem cells, Tissue Eng. Part B Rev. 22 (2016) 160–171.
[6] M. Deng, T. Mei, T. Hou, K. Luo, F. Luo, A. Yang, B. Yu, H. Pang, S. Dong, J. Xu, TGFbeta3 recruits endogenous mesenchymal stem cells to initiate bone regeneration, Stem Cell Res Ther 8 (2017) 258.
[7] G.H. Zhen, C.Y. Wen, X.F. Jia, Y. Li, J.L. Crane, S.C. Mears, F.B. Askin, F.J. Frassica, W.Z. Chang, J. Yao, J.A. Carrino, A. Cosgarea, D. Artemov, Q.M. Chen, Z.H. Zhao, X.D. Zhou, L. Riley, P. Sponseller, M. Wan, W.W. Lu, X. Cao, Inhibition of TGF-beta signaling in mesenchymal stem cells of subchondral bone attenuates osteoarthritis, Nat. Med. 19 (2013) 704–712.
[8] K. Johnson, S. Zhu, M.S. Tremblay, J.N. Payette, J. Wang, L.C. Bouchez, S. Meeusen, A. Althage, C.Y. Cho, X. Wu, P.G. Schultz, A stem cell-based approach to cartilage repair, Science 336 (2012) 717–721.
[9] X. Xu, D. Shi, Y. Shen, Z. Xu, J. Dai, D. Chen, H. Teng, Q. Jiang, Full-thickness cartilage defects are repaired via a microfracture technique and intraarticular injection of the small-molecule compound kartogenin, Arthritis Res. Ther. 17 (2015) 20.
[10] W. Fan, J. Li, L. Yuan, J. Chen, Z. Wang, Y. Wang, C. Guo, X. Mo, Z. Yan, Intra-articular injection of kartogenin-conjugated polyurethane nanoparticles attenuates the progression of osteoarthritis, Drug Delivery 25 (2018) 1004–1012.
[11] Y.J. Chuah, Y. Peck, J.E.J. Lau, H.T. Heec, D.A. Wang, Hydrogel based cartilaginous tissue regeneration: recent insights and technologies, Biomater. Sci-UK 5 (2017) 613–631.
[12] J. Xu, J. Li, S. Lin, T. Wu, H. Huang, K. Zhang, Y. Sun, K.W.K. Yeung, G. Li, L. Bian, Nanocarrier-mediated codelivery of small molecular drugs and siRNA to enhance chondrogenic differentiation and suppress hypertrophy of human mesenchymal stem cells, Adv. Funct. Mater. 26 (2016) 2463–2472.
[13] L. Zheng, D. Li, W. Wang, Q. Zhang, X. Zhou, D. Liu, J. Zhang, Z. You, J. Zhang, C. He, Bilayered scaffold prepared from a kartogenin-loaded hydrogel and BMP-2-derived peptide-loaded porous nanofibrous scaffold for osteochondral defect repair, ACS Biomater. Sci. Eng. 5 (2019) 4564–4573.
[14] M. Liu, X. Zeng, C. Ma, H. Yi, Z. Ali, X. Mou, S. Li, Y. Deng, N. He, Injectable hydrogels for cartilage and bone tissue engineering, Bone Res 5 (2017) 17014.
[15] S.L. Vega, M.Y. Kwon, J.A. Burdick, Recent advances in hydrogels for cartilage tissue engineering, Eur. Cell Mater. 33 (2017) 59–75.
[16] L. Yuan, Y. Wu, Q.S. Gu, H. El-Hamshary, M. El-Newehy, X. Mo, Injectable photo crosslinked enhanced double-network hydrogels from modified sodium alginate and gelatin, Int. J. Biol. Macromol. 96 (2017) 569–577.
[17] M.P. van den Borne, N.J. Raijmakers, J. Vanlauwe, J. Victor, S.N. de Jong, J. Bellemans, D.B. Saris, International Cartilage Repair, International Cartilage Repair Society (ICRS) and Oswestry macroscopic cartilage evaluation scores validated for use in Autologous Chondrocyte Implantation (ACI) and microfracture, Osteoarthr. Cartil. 15 (2007) 1397–1402.
[18] P. Orth, H. Madry, Complex and elementary histological scoring systems for articular cartilage repair, Histol. Histopathol. 30 (2015) 911–919.
[19] B. Zhang, H. Li, L. He, Z. Han, T. Zhou, W. Zhi, X. Lu, X. Lu, J. Weng, Surface-decorated hydroxyapatite scaffold with on-demand delivery of dexamethasone and stromal cell derived factor-1 for enhanced osteogenesis, Mater. Sci. Eng. C Mater. Biol. Appl. 89 (2018) 355–370.
[20] C. Liu, X. Ma, T. Li, Q. Zhang, Kartogenin, transforming growth factor-β1 and bone morphogenetic protein-7 coordinately enhance lubricin accumulation in bone-derived mesenchymal stem cells, Cell Biol. Int. 39 (2015) 1026–1035.
[21] Y.J. Wang, R.M. Belflower, Y.F. Dong, E.M. Schwarz, R.J. O'Keefe, H. Drissi, Runx1/AML1/Cbfa2 mediates onset of mesenchymal cell differentiation toward chondrogenesis, J. Bone Miner. Res. 20 (2005) 1624–1636.
[22] W.S. Fan, J.H. Li, Y.M. Wang, J.F. Pan, S. Li, L. Zhu, C.A. Guo, Z.Q. Yan, CD105 promotes chondrogenesis of synovium-derived mesenchymal stem cells through Smad2 signaling, Biochem. Bioph. Res. Co. 474 (2016) 338–344.
[23] N. Yoshida, T. Ogata, K. Tanabe, S.H. Li, M. Nakazato, K. Kohu, T. Takafuta, S. Shapiro, Y. Ohta, M. Satake, T. Watanabe, Filamin A-bound PEBP2 beta/CBF beta is retained in the cytoplasm and prevented from functioning as a partner of the Runx1 transcription factor, Mol. Cell. Biol. 25 (2005) 1003–1012.
[24] K.E. Lim, N.R. Park, X.G. Che, M.S. Han, J.H. Jeong, S.Y. Kim, C.Y. Park, H. Akiyama, J.E. Kim, H.M. Ryoo, J.L. Stein, J.B. Lian, G.S. Stein, J.Y. Choi, Core binding factor beta of osteoblasts maintains cortical bone mass via stabilization of Runx2 in mice, J. Bone Miner. Res. 30 (2015) 715–722.
[25] N.R. Park, K.E. Lim, M.S. Han, X.G. Che, C.Y. Park, J.E. Kim, I. Taniuchi, S.C. Bae, J.Y. Choi, Core binding factor beta plays a critical role during chondrocyte differentiation, J. Cell. Physiol. 231 (2016) 162–171.
[26] X. Qin, Q. Jiang, Y. Matsuo, T. Kawane, H. Komori, T. Moriishi, I. Taniuchi, K. Ito, Y. Kawai, S. Rokutanda, S. Izumi, T. Komori, Cbfb regulates bone development by stabilizing Runx family proteins, J. Bone Miner. Res. 30 (2015) 706–714.
[27] G. Huang, K. Shigesada, K. Ito, H.J. Wee, T. Yokomizo, Y. Ito, Dimerization with PEBP2 beta protects RUNX1/AML1 from ubiquitin-proteasome-mediated degradation, EMBO J. 20 (2001) 723–733.
[28] S.K. Zaidi, A.J. Sullivan, A.J. van Wijnen, J.L. Stein, G.S. Stein, J.B. Lian, Integration of Runx and Smad regulatory signals at transcriptionally active subnuclear sites, P. Natl. Acad. Sci. USA 99 (2002) 8048–8053.
[29] X.Y. Li, L.J. Guo, Y.T. Liu, Y.Y. Su, Y.M. Xie, J. Du, J. Zhou, G. Ding, H. Wang, Y.X. Bai, Y. Liu, MicroRNA-21 promotes osteogenesis of bone marrow mesenchymal stem cells via the Smad7-Smad1/5/8-Runx2 pathway, Biochem. Bioph. Res. Co. 493 (2017) 928–933.
[30] T. Alliston, L. Choy, P. Ducy, G. Karsenty, R. Derynck, TGF-beta-induced repression of CBFA1 by Smad3 decreases cbfa1 and osteocalcin expression and inhibits osteoblast differentiation, EMBO J. 20 (2001) 2254–2272.
[31] L. Yuan, Y. Wu, J. Fang, X. Wei, Q. Gu, H. El-Hamshary, S.S. Al-Deyab, Y. Morsi, X. Mo, Modified alginate and gelatin cross-linked hydrogels for soft tissue adhesive, Artif. Cells Nanomed. Biotechnol. 45 (2017) 76–83.
[32] Y.S. Zhang, A. Khademhosseini, Advances in engineering hydrogels, Science 356 (2017) eaaf3627.
[33] K. Flegeau, R. Pace, H. Gautier, G. Rethore, J. Guicheux, C. Le Visage, P. Weiss, Toward the development of biomimetic injectable and macroporous biohydrogels for regenerative medicine, Adv. Colloid Interf. Sci. 247 (2017) 589–609.
[34] Z. Naghizadeh, A. Karkhaneh, A. Khojasteh, Self-crosslinking effect of chitosan and gelatin on alginate based hydrogels: injectable in situ forming scaffolds, Mater. Sci. Eng. C Mater. Biol. Appl. 89 (2018) 256–264.
[35] J.S. Yang, Y.J. Xie, W. He, Research progress on chemical modification of alginate: a review, Carbohydr. Polym. 84 (2011) 33–39.
[36] M.T.I. Mredha, N. Kitamura, T. Nonoyama, S. Wada, K. Goto, X. Zhang, T. Nakajima, T. Kurokawa, Y. Takagi, K. Yasuda, J.P. Gong, Anisotropic tough double network hydrogel from fish collagen and its spontaneous in vivo bonding to bone, Biomaterials 132 (2017) 85–95.
[37] X.Y. Chen, C.Q. Dong, K.C. Wei, Y.F. Yao, Q. Feng, K.Y. Zhang, F.X. Han, A.F.T. Mak, B. Li, L.M. Bian, Supramolecular hydrogels cross-linked by pre-assembled host-guest PEG cross-linkers resist excessive, ultrafast, and non-resting cyclic compression, Npg Asia Mater 10 (2018) 788–799.
[38] Z. Luo, L. Jiang, Y. Xu, H. Li, W. Xu, S. Wu, Y. Wang, Z. Tang, Y. Lv, L. Yang, Mechano growth factor (MGF) and transforming growth factor (TGF)-beta3 functionalized silk scaffolds enhance articular hyaline cartilage regeneration in rabbit model, Biomaterials 52 (2015) 463–475.
[39] X. Li, J. Ding, Z. Zhang, M. Yang, J. Yu, J. Wang, F. Chang, X. Chen, Kartogenin-incorporated thermogel supports stem cells for significant cartilage regeneration, ACS Appl. Mater. Interfaces 8 (2016) 5148–5159.
[40] X. Hu, Y. Wang, Y. Tan, J. Wang, H. Liu, Y. Wang, S. Yang, M. Shi, S. Zhao, Y. Zhang, Q. Yuan, A difunctional regeneration scaffold for knee repair based on Aptamer-directed cell recruitment, Adv. Mater. 29 (2017) 1605235.
[41] N.A. Jalili, M.K. Jaiswal, C.W. Peak, L.M. Cross, A.K. Gaharwar, Injectable nanoengineered stimuli-responsive hydrogels for on-demand and localized therapeutic delivery, Nanoscale 9 (2017) 15379–15389.
[42] X. Sun, J. Wang, Y. Wang, Q. Zhang, Collagen-based porous scaffolds containing PLGA microspheres for controlled kartogenin release in cartilage tissue engineering, Artif. Cells Nanomed. Biotechnol. 46 (2018) 1957–1966.
[43] G.R. Cai, W. Liu, Y. He, J.H. Huang, L. Duan, J.Y. Xiong, L.J. Liu, D.P. Wang, Recent advances in kartogenin for cartilage regeneration, J. Drug Target. 27 (2019) 28–32.
[44] W. Yang, Y.Y. Zheng, J. Chen, Q.Y. Zhu, L.B. Feng, Y. Lan, P. Zhu, S. Tang, R. Guo, Preparation and characterization of the collagen/cellulose nanocrystals/USPIO scaffolds loaded kartogenin for cartilage regeneration, Mater. Sci. Eng. C Mater. Biol. Appl. 99 (2019) 1362–1373.
[45] D. Shi, X. Xu, Y. Ye, K. Song, Y. Cheng, J. Di, Q. Hu, J. Li, H. Ju, Q. Jiang, Z. Gu,

Photo-cross-linked scaffold with kartogenin-encapsulated nanoparticles for cartilage regeneration, ACS Nano 10 (2016) 1292–1299.
[46] Z.F. Jia, S.J. Wang, Y.J. Liang, Q.S. Liu, Combination of kartogenin and transforming growth factor-beta 3 supports synovial fluid-derived mesenchymal stem cell-based cartilage regeneration, Am. J. Transl. Res. 11 (2019) 2056–2069.
[47] Y. Li, T. Li, C. Liu, X.Q. Ma, Z.Y. Zhou, Z.H. Lou, J.H. Wang, Q.Q. Zhang, Induction of lubricin by kartogenin and growth factors in three-dimensional hydrogels, J. Biomater. Tissue Eng. 9 (2019) 504–510.